J|A|C|S ARTICLES

Published on Web 12/21/2009

Compressing the Most Hydrogen-Rich Inorganic Ion

Georgios Markopoulos,[†,||] Peter Kroll,[‡] and Roald Hoffmann*[,§]

Theoretische Chemie, Physikalisch-Chemisches Institut, Universität Heidelberg, Heidelberg, Germany; Department of Chemistry and Biochemistry, The University of Texas at Arlington, Arlington, Texas, United States of America; and Department of Chemistry and Chemical Biology, Baker Laboratory, Cornell University, Ithaca, New York 14853, United States of America

Received October 1, 2009; E-mail: rh34@cornell.edu

Abstract: Motivated by the potential high-temperature superconductivity of "chemically precompressed" hydrogen-rich compounds, the high pressure phases of the ionic salt $BaReH_9$ are explored theoretically. We find that the compound adapts to compression not only by structural distortions or increase of coordination number, but also through evolution of discrete H_2 units which fill up interspace gaps. This last structural change is associated with a dramatic lowering of metallization pressure, so that $BaReH_9$ can be expected to turn metallic at the onset of the H_2-containing phase (51 GPa).

Introduction

Matter changes dramatically under the influence of pressure, giving rise to a plethora of unusual properties and phenomena.[1−4] Among them is the pressure-induced metallization of materials that are insulating covalent, ionic, or molecular solids, even gases, at ambient pressure. In this context, solid metallic hydrogen is keenly awaited in the high pressure community, as it is predicted to be a high-temperature superconductor.[5] So far, pressures of up to 342 GPa were not sufficient to achieve its metallization, even as the band gap in the material is much reduced.[6] It has been argued that compression of hydrogen-rich molecular compounds might also be a way to high-temperature superconductivity—at pressures much lower than those necessary for pure hydrogen.[7] One can think of hydrogen as being "chemically precompressed" in such hydrides. Another way to look at this is to consider the intramolecular H···H separation in a molecule such as EH_4 (E = Group 14 element): that distance is substantially closer than the H···H van der Waals contact. Indeed, SiH_4 has been predicted to metallize at pressures of the order of 100 GPa.[8] And recently, a T_c of = 17 K has been experimentally observed in compressed silane at 96 and 120 GPa.[9]

Motivated by the ideas just presented, we examine theoretically in this contribution the high-pressure phases of the hydrogen-rich compound $BaReH_9$. The ReH_9^{2-} anion in this ionic salt features one of the highest metal-to-hydrogen atomic ratios known.[10] Also, the hydrogen density of $BaReH_9$ at atmospheric pressure amounts to 134 g/L, which is approximately twice that of liquid hydrogen—[11]in and of itself a striking example of "chemical precompression". Starting from the observed NiAs-type structure of $BaReH_9$ at ambient pressure, in this work we explore computationally potential structures as the pressure increases. As we will see, at elevated pressures, a novel structure containing distinct H_2 molecules and Re polyhydride chains emerges. We study the electronic structure of the $BaReH_9$ phases as a function of pressure, paying special attention to metallization. The computational methodology is specified in the Appendix.

Results and Discussion

NiAs-type $BaReH_9$ Structure at Ambient and Elevated Pressure. At atmospheric pressure, $BaReH_9$ crystallizes in a hexagonal structure ($P6_3/mmc$).[11] Focusing on the heavy atoms only, the structure resembles the NiAs-type. The hydrogen positions could not be refined in the cited study, but two neutron diffraction structures on the related salt K_2ReH_9 located the hydrogens of the complex anion ReH_9^{2-}.[12,13] Their tricapped-prismatic arrangement with D_{3h} symmetry was also assumed for our calculations. Each ReH_9 unit itself is coordinated by 6 barium ions forming a trigonal prism (Figure 1).

Our calculations at ambient pressure reproduced the experimental structure nicely (details in Supporting Information). We

[†] Theoretische Chemie, Physikalisch-Chemisches Institut, Universität Heidelberg.

[‡] Department of Chemistry and Biochemistry, The University of Texas at Arlington.

[§] Department of Chemistry and Chemical Biology, Cornell University.

[||] Current address: Institut für Organische Chemie, Technische Universität Braunschweig, Braunschweig, Germany.

(1) Holzapfel, W. B. *Rep. Prog. Phys.* **1996**, *59*, 29–90.
(2) Hemley, R. J. *Annu. Rev. Phys. Chem.* **2000**, *51*, 763–800.
(3) McMillan, P. F. *Chem. Soc. Rev.* **2006**, *35*, 855–857.
(4) Grochala, W.; Hoffmann, R.; Feng, J.; Ashcroft, N. W. *Angew. Chem., Int. Ed.* **2007**, *46*, 3620–3642.
(5) Ashcroft, N. W. *Phys. Rev. Lett.* **1968**, *21*, 1748–1749.
(6) Narayana, C.; Luo, H.; Orloff, J.; Ruoff, A. L. *Nature* **1998**, *393*, 46–49.
(7) Ashcroft, N. W. *Phys. Rev. Lett.* **2004**, *92*, 187002.
(8) Feng, J.; Grochala, W.; Jaron, T.; Hoffmann, R.; Bergara, A.; Ashcroft, N. W. *Phys. Rev. Lett.* **2006**, *96*, 17006.
(9) Eremets, M. I.; Trojan, I. A.; Medvedev, S. A.; Tse, J. S.; Yao, Y. *Science* **2008**, *319*, 1506–1509.
(10) Wang, X.; Andrews, L.; Infante, I.; Gagliardi, L. *J. Am. Chem. Soc.* **2008**, *130*, 1972–1978.
(11) Stetson, N. T.; Yvon, K.; Fischer, P. *Inorg. Chem.* **1994**, *33*, 4598–4599.
(12) Abrahams, S. C.; Ginsberg, A. P.; Knox, K. *Inorg. Chem.* **1964**, *3*, 558–567.
(13) Bronger, W.; à Brassard, L.; Müller, P.; Lebech, B.; Schultz, T. *Z. Anorg. Allg. Chem.* **1999**, *625*, 1143–1146.

 10.1021/ja908345e

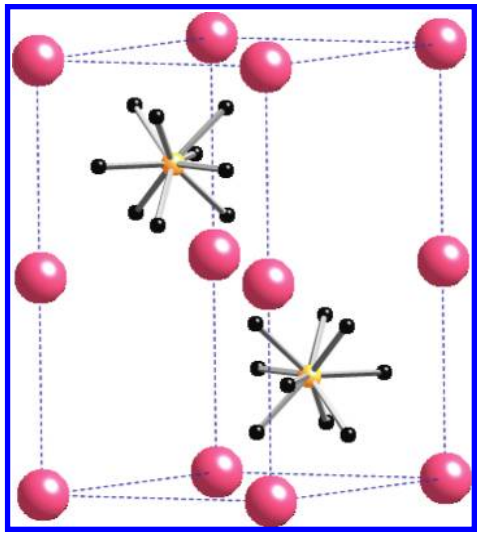

Figure 1. NiAs-type BaReH$_9$ at ambient pressure ($P6_3/mmc$, $Z = 2$; Ba = rose, Re = yellow, H = black).

Table 1. Structural Parameters and Shortest Distances in Å for NiAs-Type BaReH$_9$ at Ambient Pressure and Metallization[a,b]

pressure [GPa]	0	115
volume per BaReH$_9$ [Å^3]	115.7	55.3
V/V_0	1.0	0.48
$a = b$	5.25	3.96
c	9.70	8.14
ratio c/a	1.85	2.06
Ba−Ba	4.85	3.96
Re−Ba	3.88	3.06
Re−Re	5.25	3.96
Ba−H	2.78	2.16
Re−H$_a$ (see footnote *c*)	1.68	1.56
Re−H$_b$ (see footnote *c*)	1.71	1.66
H−H (within ReH$_9$)	1.92	1.77
H−H (between ReH$_9$)	2.35	1.26
∠ H$_b$−Re−H$_b$′	89.4°	76.5°

[a] Distances are reported in Å. [b] For comparison, we give standard radii from ref 22 Ba^{2+} (ionic radius) = 1.43 Å; Re (metallic radius) = 1.37 Å; H (covalent radius) = 0.37 Å). [c] H$_a$ refers to the three equivalent H that form the caps; H$_b$ to the six equivalent H that form the prism, respectively.

determined the band gap as 3.85 eV, although it should be kept in mind that DFT methods typically underestimate the band gap.[14] Singh et al. calculated a band gap of 3.58 eV within the LDA approximation.[15] If the NiAs-type structure is constrained to retain point group symmetry D_{3h}, then metallization is achieved at 115 GPa. This reflects a compression to approximately 48% of the initial volume.

Structural parameters for the compressed structure are given in Table 1. The Re−H bond lengths (shortened by 3−7%) are significantly less affected than other distances (18−24%); this reflects the strength of the covalent bond as well as the fact that van der Waals space is most easily squeezed out. Also, angle deformation along the c-direction seems to offer an energetically less costly way for compression; electronic effects of this deformation will be discussed later. Furthermore, we wish to emphasize the short intermolecular H···H separation between ReH$_9$ units (1.27 Å) in the compressed structure, as this is a first hint to the future evolution of H$_2$ units.

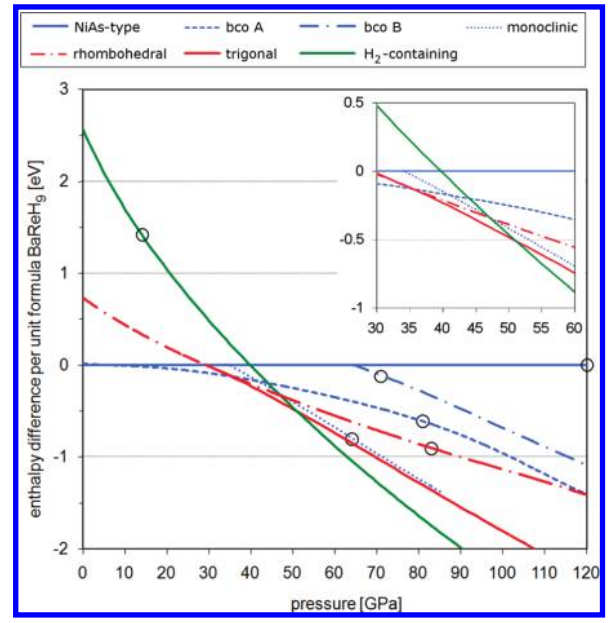

Figure 2. Thermodynamic stability of investigated structures: the arbitrary zero of enthalpy is the NiAs-type structure. Blue structures are distortions thereof, red structures are derived from the CsCl-type, green structure contains H$_2$ units. Black circles indicate metallization.

There might also be a concern about nonclassical H···H bonding, an exciting phenomenon in the organometallic chemistry of the last two decades.[16−20] The occurrence of this in ambient pressure BaReH$_9$ has already been discussed by Parker et al., who argued against it.[21] Even for compression down to 47% of the initial volume, we observe a minimum intramolecular H···H separation of 1.77 Å within the ReH$_9$ units. This is well above the value for side-on bonded dihydrogen complexes (<1.0 Å) or even stretched dihydrogen complexes (<1.6 Å).[17]

Deformations of the NiAs-Type Structure with Increasing Pressure. As we moved to higher pressure, we encountered and explored a variety of structures, some closely related to the NiAs-type structure, some quite different from it. We will discuss them in turn, but give an overview of their thermodynamic stability first (Figure 2).[23] Nothing is simple in the high pressure world, and in the range of 10−60 GPa, we found five structures that are more stable than the NiAs-type structure. All except the H$_2$-containing structures, which we are going to discuss in substantial detail below, retain distinct molecular ReH$_9$ entities. At around 45 GPa, the five structures are of comparable enthalpy; given what we know of the computational methodology (DFT), we would not risk a prediction of one of these being most stable in this intermediate pressure range.

Starting from ambient pressure, the NiAs-type structure remains competitive up to 4 GPa. For pressures between 4−35

(14) Städele, M.; Moukara, M.; Majewski, J. A.; Vogl, P.; Görling, A. *Phys. Rev. B* **1999**, *59*, 10031–10043.
(15) Singh, D. J.; Gupta, M.; Gupta, R. *Phys. Rev. B* **2007**, *75*, 35103.
(16) Kubas, G. J. *Chem. Rev.* **2007**, *107*, 4152–4205.
(17) Maseras, F.; Lledos, A.; Clot, E.; Eisenstein, O. *Chem. Rev.* **2000**, *100*, 601–636.
(18) Heinekey, D. M.; Oldham, W. J. *Chem. Rev.* **1993**, *93*, 913–926.
(19) Jessop, P. G.; Morris, R. H. *Coord. Chem. Rev.* **1992**, *121*, 155–284.
(20) Crabtree, R. H. *Angew. Chem., Int. Ed.* **1993**, *32*, 789–805.
(21) Parker, S. F.; Refson, K.; Williams, K. P. J.; Braden, D. A.; Hudson, B. S.; Yvon, K. *Inorg. Chem.* **2006**, *45*, 10951–10957.
(22) Emsley, J. *The Elements*; Repr. (with corr.); Clarendon Press: Oxford, 1990.
(23) Essential structures have also been calculated at the LDA level of theory. The energetic ordering remains unchanged, but transition pressures are 1−6 GPa lower. Please refer to Supporting Information for details.

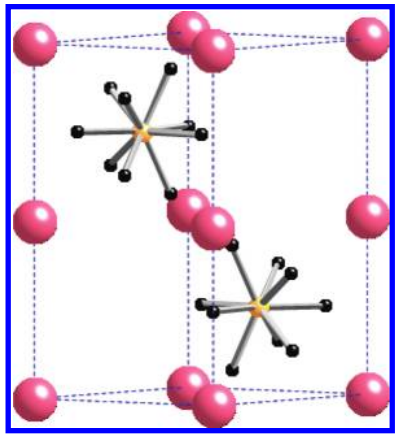

Figure 3. Base-centered orthorhombic structure A at 27 GPa (*Cmcm*).

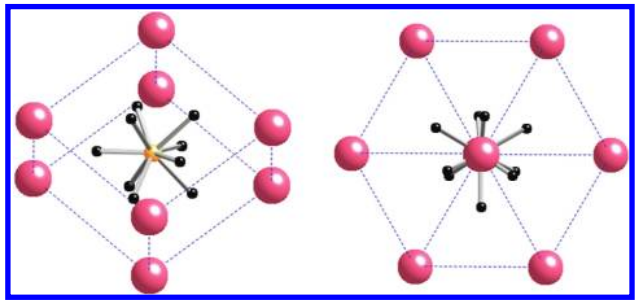

Figure 4. Two views of rhombohedral structure at ambient pressure (*R*32, $Z = 1$).

GPa we find the *base-centered orthorhombic structure A* as the enthalpically most stable. It constitutes a distortion from the NiAs-type; the ReH_9 units are still coordinated by 6 bariums ions, but adopt a molecular C_{2v} symmetry (Figure 3). In inorganic chemistry, nine-coordination is a pretty flexible geometry[12] and it seems that the material adjusts to pressurization by deformation of the ReH_9^{2-} ion. Indeed, one could almost argue that the tricapped prism realigns along the *xy*-plane. Two other distortions (*monoclinic structure* and *base-centered orthorhombic structure B*), which cannot compete with other high pressure phases, are shown in the Supporting Information. All these distortions show a significantly lower metallization pressure than their parent structure (see black circles in Figure 2). This might be related to crystal packing effects, but also to electronic changes (to be discussed below) due to the observed deformations.

Increase of Coordination Number. Looking for further high pressure phases besides those which develop as continuous distortions of the parent NiAs-type structure, we exploited the richness of higher coordinated AB-type structures ($A = Ba^{2+}$, $B = ReH_9^{2-}$). Among these, we set up a CsCl-type structure: the ReH_9^{2-} anion was aligned along the unit cell diagonal, and subsequent relaxation under C_3-symmetry constraint yielded a *rhombohedral structure* (Figure 4). At ambient pressure, this hypothetical phase is 4% denser than the NiAs-type structure; its band gap was calculated as 3.13 eV (compared to 3.85 eV for the NiAs-type structure). Closest distances and ReH_9 geometry correspond well with the NiAs-type, the Re···Re distance alone is smaller. As we show in Figure 4, the ReH_9 prism is slightly twisted (8°). This deformation is reminiscent of the Bailar twist in trigonal prismatic ML_6 complexes[24] and

(24) Bailar, J. C. *J. Inorg. Nucl. Chem.* **1958**, *8*, 165–175.

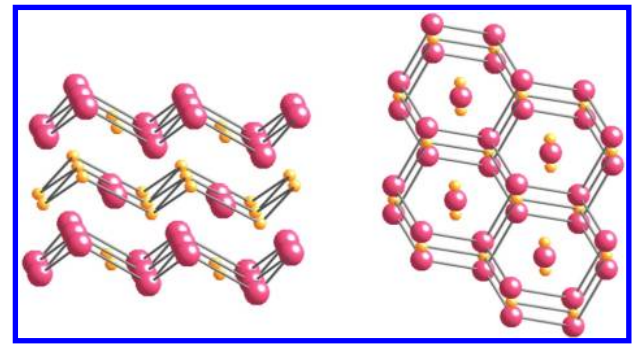

Figure 5. Two views of trigonal structure at 42 GPa (*P*3, $Z = 3$). Hydrogen atoms are not displayed; several unit cells are shown to emphasize the overall structure.

amounts to 17° at the metallization pressure (77 GPa). Also, the H_b-Re-H_b' angle is widened at metallization, in contrast to the corresponding decrease in NiAs-type $BaReH_9$.

The rhombohedral structure would be the most stable structure for pressures around 40 GPa, were a distortion not possible. This was found by using a supercell approach. Setting up the rhombohedral structure in a trigonal unit cell with 3 formula units $BaReH_9$, allowed for a more diversified structure upon compression: we observed a translocation along the *c*-axis, which rendered the various Ba and Re centers inequivalent. This modified structure turned out to be the enthalpically most stable one in the pressure range between 35−51 GPa; below 35 GPa, it optimized back to the rhombohedral structure.

The *trigonal structure* at 42 GPa is presented in Figure 5. For the sake of clarity, we begin without showing the hydrogen atoms; their arrangement will be discussed later. The Ba ions are assembled in wavy sheets of six-membered rings, comparable to the classical three-connected structure of gray arsenic. A second set of Ba ions is interdispersed. At 42 GPa, the Ba···Ba distance within the rings is 3.85 Å (for comparison, ionic radius of $Ba^{2+} = 1.43$ Å); the distances to an isolated Ba ion range between 4.06−5.21 Å. The Re centers are arranged in a corresponding fashion, although they are not in direct contact with each other due to the coordinating hydrogen atoms. The latter essentially maintain the C_3-symmetric arrangement of the rhombohedral structure, although the hydrogen atoms denoted as H_a (see footnote (c) to Table 1) are increasingly pushed out of the intersecting plane.

Much to our surprise, this structure did not turn metallic for pressures up to 121 GPa, where we still observed a band gap of 0.85 eV. We also observed a symmetry reduction to a *triclinic structure*, which becomes energetically favorable beyond 80 GPa. The respective changes in the lattice parameters are small with respect to the initial structure (angle deformations do not exceed 2−3°; lengths of the lattice vectors remain essentially constant).

New Structural Types, Containing Discrete H_2 Units. Discrete ReH_9^{2-} motifs dominate the structures of $BaReH_9$ below 51 GPa. This changes now, as the pressure is elevated. At very high compressions, the NiAs-type structure and its various distortions exhibited remarkably short intermolecular H···H contacts, which in our calculations easily led to a new structure with discrete H_2 units. Indeed, we have found two closely related variants of this motif. Both are monoclinic, but differ in their stereochemical arrangement. One of them is shown at 52 GPa in Figure 6, the other variant is described in the SI. Their energy difference is less than 0.01 eV, making a prediction of their relative stability impossible. More importantly, these H_2-

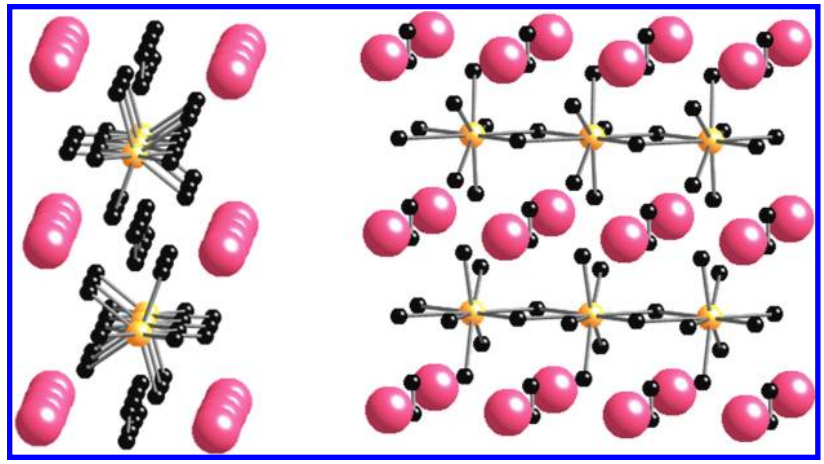

Figure 6. Front and side view of H_2-containing structure at 52 GPa ($P2_1/m$, $Z = 2$). Unit cell repeated to emphasize polymeric chains. This figure shows the variant which we are going to denote "eclipsed" in the Supporting Information.

containing structures turned out to be the most stable phase for pressures beyond 51 GPa.

The striking structural feature we see is of H_2 units along with polymeric $[ReH_7^{2-}]_n$ chains. At 52 GPa, the H···H distance within the H_2 units amounts to 0.79 Å, which is slightly larger than that of gaseous H_2 (0.74 Å). Every H_2 unit itself is at least 2.28 Å away from the closest rhenium center; contrastingly, the Re···H distances within the $[ReH_7^{2-}]_n$ polymers range between 1.64−1.94 Å (standard Re−H bond lengths are usually around 1.70 Å). These polymeric chains consist of almost planar ReH_5 units, sharing four hydrogen atoms with adjacent rhenium centers; the bridging hydrogens are not symmetrically sandwiched between the ReH_5 units.

Our calculations on the H_2-containing structures also revealed some variability in the position of the discrete H_2 units: small displacements and rotations were possible without significant energetic consequences. This suggested that the $BaReH_7$ backbone is in a way quite independent from the H_2 units. However, it should be pointed out that the respective Ba···H_2 separation (2.25 Å) in this compressive regime is shorter than the ambient pressure Ba···H distance in the ionic hydride BaH_2 (2.5−3.0 Å).[25] Also, the Ba···Ba separation (3.12 Å) is close to the hard sphere contact of two barium ions, assuming a Ba^{2+} radius of 1.43 Å.[22] Considering the bonding along the polymeric chains, we observed a Re···Re distance of 3.12 Å. This value is well above the Re···Re distance in metallic Re, which exhibits a radius of 1.37 Å. However, if we consider the empirical covalent radius of Re to be 1.51 Å,[26] then we get well into the range of a bonding interaction. For example, the Re−Re bond in $Re_2(CO)_{10}$ at ambient pressure amounts to 3.04 Å.[27] Also, a nice analogy is at hand with polymeric $[ReH(CO)_4]_n$, which exhibits a single bridging hydrogen and an Re···Re distance of 3.3−3.4 Å.[28]

The substantially different topology of the H_2-containing phase is associated with a prominent change in electronic structure: the band gap at ambient pressure was calculated as 0.34 eV, which is about 3 eV less than for NiAs-type $BaReH_9$; the metallization pressure drops as low as 14 GPa—a region where this structure is not yet the most stable one. We will explain these findings at the end of the present contribution, unfolding the details of band-overlap metallization in $BaReH_9$.

For the low pressure regime we have found an additional H_2-containing structure with ReH_6 units and single bridging hydrogen (see Supporting Information). At ambient pressure, this structure is about 0.17 eV more stable than the other H_2-containing structures; it remains energetically preferred to them for pressures up to 14 GPa. But there are other more stable (non-H_2-containing) structures in this pressure range.

Generally, the evolution of discrete H_2 units under compression is unusual; it is reported only in two computational studies on high pressure SnH_4 and GeH_4.[29,30] We have also observed it in our group in unpublished work (P. Gonzalez-Morelos and R. H.) on another SnH_4 structure. Obviously, the H_2 units allow denser packing (at least for a while, as the pressure increases)—albeit at cost of electronic energy: at ambient pressure, the H_2-containing structure is about 15% denser than the NiAs-type $BaReH_9$, but 2.56 eV higher in energy.

The electronic cost of hydrogen evolution at ambient pressure is also reflected in the corresponding reaction of discrete molecules, $ReH_9^{2-} \rightarrow H_2 + ReH_7^{2-}$, for which we calculated an unfavorable $\Delta E = 1.56$ eV.[31] Still, H_2-containing $BaReH_9$ becomes competitive at high pressures, as the pV term in the enthalpy $H = E + pV$ overcomes the electronic impediment.

Concerning the experimental feasibility of an H_2-containing phase, it is important to consider whether gaseous hydrogen could escape. Inspection of the phase diagram of H_2 reveals that this is unlikely: hydrogen is solid over a wide range of temperatures in the pressure region of interest ($p > 40$ GPa).[32]

We have also studied the decomposition into solid H_2 and hypothetical $BaReH_7$ for pressures beyond 40 GPa. As a

(25) Bronger, W.; Scha, Chi-Chien; Müller, P. *Z. Anorg. Allg. Chem.* **1987**, *545*, 69–74.
(26) Cordero, B.; Gomez, V.; Platero-Prats, A. E.; Reves, M.; Echeverria, J.; Cremades, E.; Barragan, F.; Alvarez, S. *Dalton Trans.* **2008**, 2832–2838.
(27) Churchill, M. R.; Amoh, K. N.; Wasserman, H. *J. Inorg. Chem.* **1981**, *20*, 1609–1611.
(28) Masciocchi, N.; D'Alfonso, G.; Garavaglia, L.; Sironi, A. *Angew. Chem., Int. Ed.* **2000**, *39*, 4477–4480.
(29) Tse, J. S.; Yao, Y.; Tanaka, K. *Phys. Rev. Lett.* **2007**, *98*, 117004.
(30) Gao, G.; Oganov, A. R.; Bergara, A.; Martinez-Canales, M.; Cui, T.; Iitaka, T.; Ma, Y.; Zou, G. *Phys. Rev. Lett.* **2008**, *101*, 107002.
(31) We report electronic energies without any zero-point energy correction. The activation energy has not been computed, nor the question examined whether this elimination is symmetry allowed. The reported ΔE is based on the singlet state of ReH_7^{2-}. Actually, the triplet state is more stable by about 0.29 eV (see Supporting Information).
(32) Bonev, S. A.; Schwegler, E.; Ogitsu, T.; Galli, G. *Nature* **2004**, *431*, 669–672.

computational model for solid H_2, we used the $P6_3/m$ structure of Pickard and Needs.[33] For $BaReH_7$ we did not perform as exhaustive a structure optimization as for $BaReH_9$. Rather, we used the $BaReH_7$ backbone of the H_2-containing structures as an initial guess and optimized this motif. Starting from the variant given in the Supporting Information, a stable structure was obtained that kept the $BaReH_7$ backbone essentially intact. However, if we began with the H_2-containing variant shown in Figure 6, a substantial distortion took place and a modification with significantly lower energy evolved. In both cases, the reaction enthalpy for the decomposition $BaReH_9 \rightarrow BaReH_7 + H_2$ turned out positive and increasing with pressure: in the pressure region of interest (40−90 GPa), the value ranges from 0.3−0.8 eV for "conserved" $BaReH_7$ and around 0.05 eV for "distorted" $BaReH_7$ (see Supporting Information). The smallness of this latter value prevents us from drawing final conclusions on a decomposition of $BaReH_9$. While further influence of pressure and temperature on the Gibbs energy may favor it, low temperatures may kinetically stabilize $BaReH_9$. The zero-point motion of hydrogen was not considered at this point and would require further computational investigations.

The impressive stability of H_2-containing $BaReH_9$ in the high pressure regime motivated us to explore this motif further: Can the introduction of a second hydrogen molecule lead to even denser packing? How big will the electronic cost be? The Supporting Information to this work considers three hypothetical structures with two or three H_2 molecules per Re. None competes energetically with the structures we have seen so far. Neither do two structures of high symmetry with a nonmolecular distribution of hydrogen.

Pressure-Induced Metallization of $BaReH_9$. The high pressure behavior of $BaReH_9$ presented us with several competing effects. First, we observed that pressure may distort the original structure. This is the case at 4 GPa, when the hexagonal NiAs-type distorts into an orthorhombic modification. Second, a rather classical coordination increase occurs at 36 GPa, when the structure transforms from the NiAs-type to CsCl-type. Third, we observed the rather unusual evolution of H_2 units. This process, which a chemist would call a reductive elimination, is remarkable, as it is associated with a chemically less favorable local bonding situation at Re. At high pressures, density rules—more favorable packing is the driving force for this structural change.

In what follows, we wish to shed some light on the mechanism of pressure-induced metallization in $BaReH_9$. Figure 7 shows the band structure and projected density of states (DOS) for NiAs-type $BaReH_9$ at ambient pressure. Its electronic structure has recently been discussed in extensive detail by Singh et al.[15] In summary, the bands from −6 to 0 eV arise from the bonding molecular orbitals of the constituent ReH_9^{2-} ion; the two bands around −5.5 eV in particular come from the totally symmetric A_1' combination of the Re 6*s* and H 1*s* orbitals. There are two formula units of $BaReH_9$ per unit cell, therefore the number of bands is doubled. We also show the subvalence Ba 5*p* bands at −11 eV, as they will become more prominent upon compression. With some reservations about the ability of the software to partition DOS properly, we identify the conduction band as a mixture of Ba 5*d* and Re−H antibonding states.

Metallization of the NiAs-type structure sets in at 115 GPa and we give the respective DOS in Figure 8. The gap between the Ba 5*p* and Re−H states has closed, as has the gap within

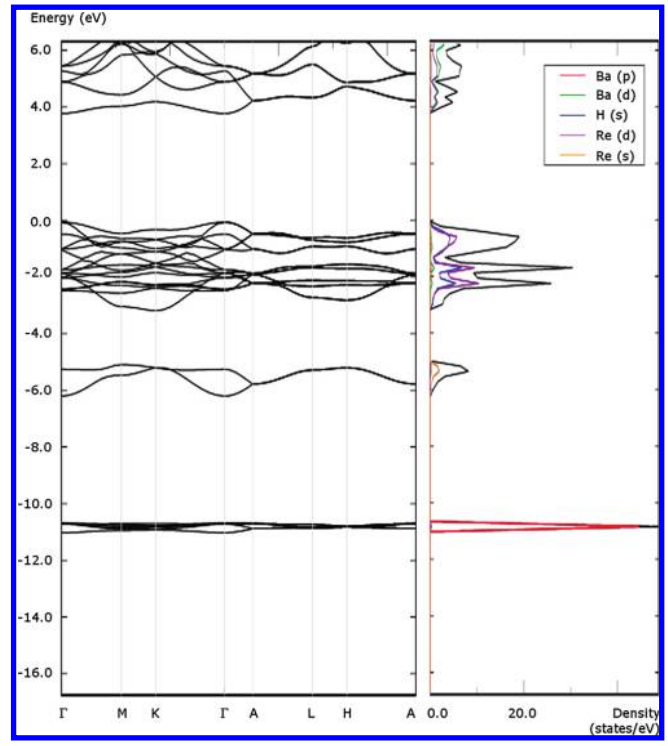

Figure 7. Band structure and projected DOS for NiAs-type $BaReH_9$ at ambient pressure. As pointed out in the Methods section, the projected densities of states are not normalized.

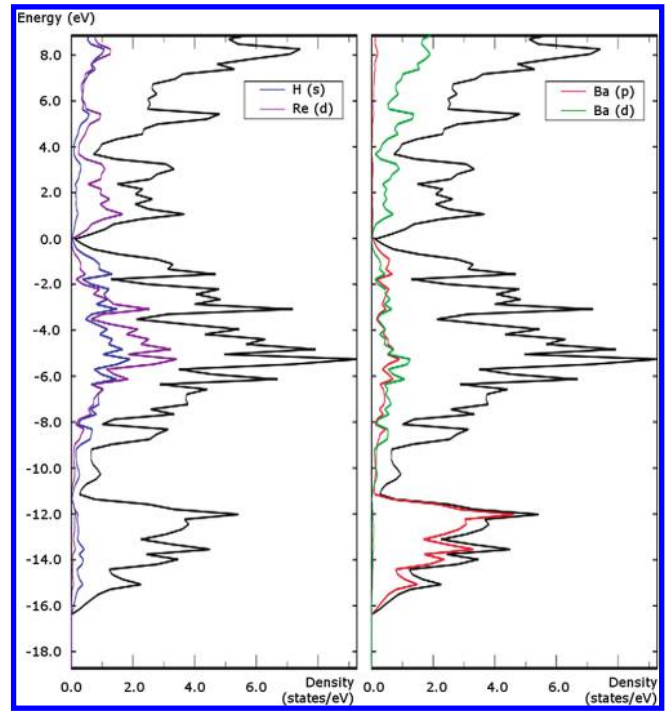

Figure 8. Projected DOS for NiAs-type structure at metallization (115 GPa).

the Re−H states. The states around the Fermi level (which we always set to 0 eV; we also set here and elsewhere the Fermi level at the energy of the highest point of the valence band; rigorously, it should lie halfway between the valence and conduction band) have Re−H character, although there is also widespread contribution of Ba 5*d* and some Ba 5*p*. We have further calculated the ionic sublattices of Ba^{2+} and

(33) Pickard, C. J.; Needs, R. J. *Nature Phys.* **2007**, *3*, 473–476.

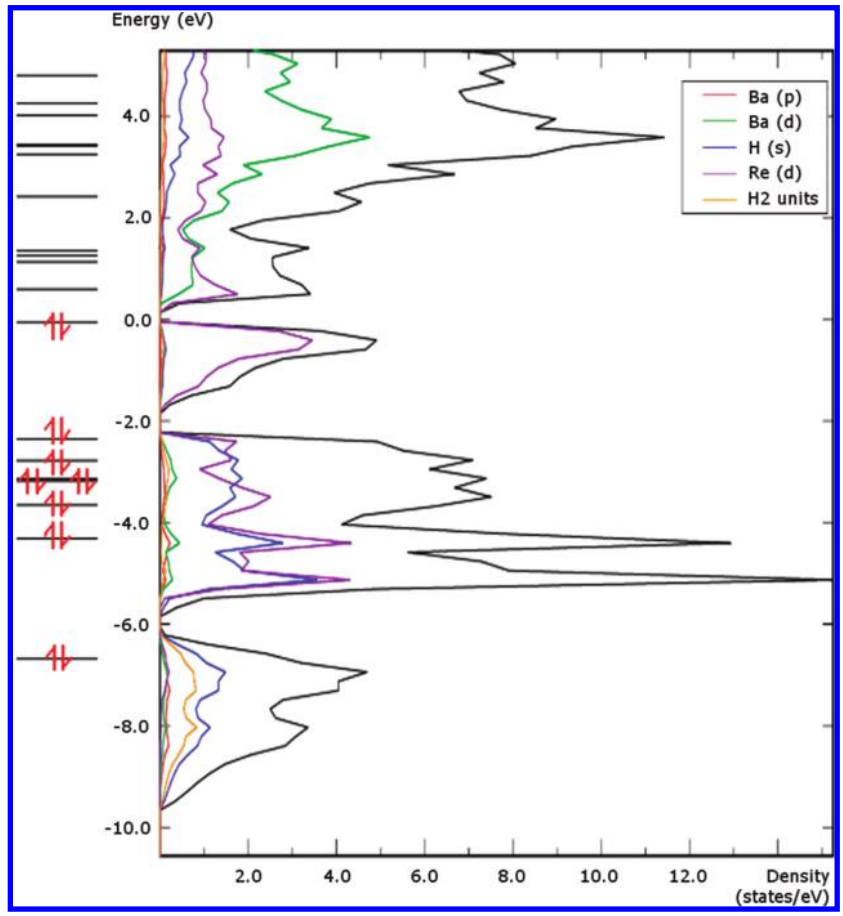

Figure 9. Projected DOS for H_2-containing structure (the "staggered" variant described in the Supporting Information; subvalence Ba 5p levels not shown this time) at ambient pressure. On the left, energy levels of the constituent ReH_7^{2-} anion with HOMO energy set to 0 eV. The molecule levels come from a single-point calculation on discrete ReH_7^{2-} ion at the B3LYP level of theory.

ReH_9^{2-} at this pressure (these are given in the Supporting Information, as are more detailed Ba, Re, and H projections): they indicate band gap closure for the ReH_9^{2-} sublattice; the Ba 5*d* states as well as a small Ba 6*s* contribution appear slightly above the Fermi level. The Ba 5*p* states in this sublattice appear as a sharp peak, which in the complete structure interact fairly strongly with the low-energy Re−H states. However, the computational reliability of ionic sublattice calculations is not guaranteed, as we calculate charged species with long-range Coulomb interactions under periodic boundary conditions.[21,34]

The above analysis for NiAs-type $BaReH_9$ revealed that filled Re−H bonding states are involved in band gap closure; they overlap with a mix of empty Re−H antibonding and Ba 5*d* states. This suggests that metallization might not only be related to greater band dispersion, but also to an energy shift of the highest occupied molecular orbital (HOMO) of the ReH_9^{2-} ion due to structural deformation. For example, compression of the Re−H bond is expected to increase the HOMO energy. Moreover, we observed a reduced H_b−Re−$H_{b'}$ angle upon compression (cf. Table 1). A Walsh diagram (given in the Supporting Information) from a simple extended Hückel calculation demonstrates that this angular deformation indeed leads to a rise in HOMO energy as well as a lowering of the lowest unoccupied molecular orbital (LUMO). Similar effects on the electronic structure are expected for the distortions of NiAs-type $BaReH_9$ as well as for the rhombohedral and trigonal structures mentioned above. These geometries are the most stable ones in the range of 4−51 GPa, but their metallization pressures lie well above their region of stability. Transfer of electrons from bonding to antibonding Re−H states should also affect the respective Re−H bond length: an increase of the Re−H distance should be observed. However, this effect is hard to quantify as increasing metallization requires higher compression. The latter, of course, opposes the described effect.

The H_2-containing phase exhibits a remarkably low metallization pressure of 14 GPa. Also, its band gap at ambient pressure was calculated as only 0.34 eV. These findings can be understood by analysis of the ReH_7^{2-} entity which constitutes the building block of the polymeric $[ReH_7^{2-}]_n$ chains. Qualitative molecular orbital theory predicts 7 bonding, 2 nonbonding, and 7 antibonding molecular orbitals (MO) for discrete ReH_7^{2-}. The respective energy levels from a DFT calculation are shown on the left-hand side of Figure 9 (HOMO energy set to 0 eV).[35] As we consider what in the organometallic trade would be called a 16-electron complex, only one of the nonbonding MO will be occupied.[36]

The electronic structure of the molecular anion transfers nicely to the solid state material: below the Fermi level one sees a dominant Re(d) peak. This is also consistent with what happens from an organometallic perspective—the formation of H_2, formally an oxidative coupling, is accomplished by

(34) Martin, R. M. *Electronic Structure—Basic Theory and Practical Methods*; Cambridge University Press: Cambridge, 2004; p 56.
(35) In molecular calculations we use the B3LYP functional, which appears better suited to the problem.

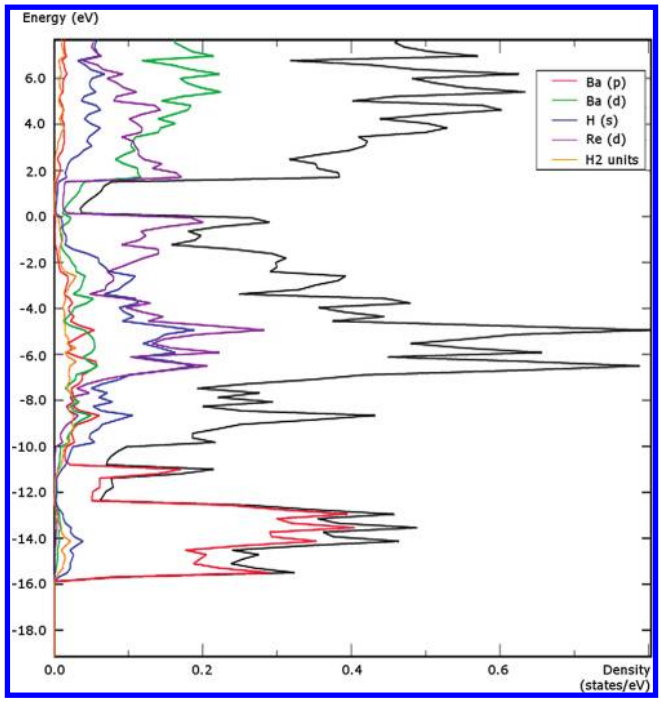

Figure 10. Projected DOS for H_2-containing structure (the "staggered" variant in SI) at 52 GPa.

reduction of Re. The contribution of the discrete H_2 units is located between −6 and −10 eV, which also are the energy range of the lowest MO of the ReH_7^{2-} anion.[37] No H(s) contribution is found around the Fermi level, confirming the presence of nonbonding Re states. These nonbonding states, which do not exist in NiAs-type $BaReH_9$, are primarily responsible for the significantly reduced HOMO−LUMO gap of the H_2-containing phase. However, there is also a strong Ba(d) contribution just above the Fermi level.

The band structure underlying this density of states analysis is given in the Supporting Information, along with electronic structure details for the onset of metallization at 14 GPa. The DOS at 52 GPa, at which the H_2-containing phase becomes enthalpically competitive, is shown in Figure 10. We clearly see a density at the Fermi level, rich in Re(d) character below and Ba(d) character above the Fermi level. Metallization is obviously due to band overlap between nonbonding Re states and empty Ba(d) states. The H_2 entities are not involved in band gap closure.

Conclusions

We predict a variety of structural changes for high-pressure $BaReH_9$. Most interestingly, a metallic phase with polymeric $[ReH_7^{2-}]_n$ chains and discrete H_2 units is expected for pressures beyond 51 GPa. Our results cannot exhaustively exclude the possibility of decomposition, but this high-pressure motif, arising in a different way in SnH_4 and GeH_4, might still have some generality: it should form part of the thinking around the structures of any other compounds where small diatomics can evolve, for example halogen-rich clusters. And it should be considered for transition-metal systems where a reductive elimination is not favored at low pressure (yet might become competitive at high pressure).

The surprisingly low metallization pressure of the H_2-containing phase (14 GPa) lies well below the pressure at which this structure type becomes enthalpically favorable. Our prediction of metallization in $BaReH_9$ is therefore not associated with the traditional "band gap problem" of DFT methods.[34] Furthermore, the onset of a metallic phase at 51 GPa is exciting with respect to potential high-temperature superconductivity—which might be additionally enhanced by the presence of the discrete H_2 units.[30] One should try to squeeze $BaReH_9$.

Appendix: Computational Methods

Solid state calculations were performed with the Vienna ab initio simulation package (VASP), which is a plane-wave code for density functional theory (DFT) calculations on extended materials.[38,39] We used the GGA functional by Perdew, Becke and Ernzerhof (PBE),[40] which has been found to be reliable for the prediction of pressure-induced phase transitions.[41,39] Atomic potentials were based on the projector-augmented wave method (PAW).[42,43] For Rhenium, the 5*p*, 6*s*, and 5*d* states were treated as valence states; for barium, the 5*s*, 5*p*, and 6*s* states, respectively. The energy cutoff for the plane-wave basis was set to 500 eV. Selected structures were also calculated at the LDA level of theory (LDA = Local Density Approximation). The respective data can be found in the Supporting Information.

Integrals over the Brillouin zone were performed with k-point grids generated via the Monkhorst-Pack scheme.[44] The number of divisions along each reciprocal lattice vector of a structure was chosen such as to provide an energy convergence of <0.001 eV/atom. The following setting was usually found to be sufficient: (divisions along reciprocal lattice vector) times (corresponding lattice constant) = 15 − 25 Å. For density of states (DOS) calculations and band gap determinations, the number of divisions was usually multiplied by 3. We generally used the Gaussian smearing method with the width of smearing set to 0.2 eV. At the onset of metallization, this value was usually adjusted to 0.02 eV in order to guarantee an accurate extrapolation of the energy to zero smearing. Metallization pressures were determined in intervals of 4−7 GPa. However, it is important to note that DFT typically underestimates the band gap.[14] Experimental metallization pressures may therefore be higher than predicted by our study. Reported energies always refer to one formula unit $BaReH_9$.

Structural relaxations involved the optimization of unit cell vectors and atomic positions. Structures were optimized until the maximum residual force component was smaller than 0.005 eV/Å; for some structures a value of 0.010 eV/Å was employed. Both settings guaranteed an energy convergence of <0.001 eV/atom. For high pressure calculations, we fixed the unit cell

(36) A triplet state is also possible and is indeed favored by 0.46 eV (see Supporting Information). This would result in a solid state magnetic insulator for the extended material. To study this possibility would require further computational investigations. However, a hypothetical magnetic insulating phase would not change our reasoning significantly. This can be seen by imagining the respective enthalpy curve in Figure 2 lowered, just as a way of estimating what a magnetic phase might do. Also, pressure usually quenches (itinerant) magnetism. Thus, we may expect the triplet state to become less favorable over the singlet at high pressures.

(37) The contributions from the antibonding MO of the H_2 units do not appear in the energy window shown; they are either high up in energy or their contribution to virtual states is underestimated. For example, a VASP calculation on a discrete H_2 molecule with the same bond length as in the H_2-containing structure at ambient pressure (0.79 Å) yields a HOMO−LUMO gap of 9.81 eV. This suggests that the contribution from the σ^* orbital of the H_2 units should appear ~2 eV above the Fermi level.

(38) Hafner, J. *Comput. Phys. Commun.* **2007**, *177*, 6–13.
(39) Hafner, J. *J. Comput. Chem.* **2008**, *29*, 2044–2078.
(40) Perdew, J. P.; Burke, K.; Ernzerhof, M. *Phys. Rev. Lett.* **1996**, *77*, 3865–3868.

volume at a certain value and allowed for structural relaxation under this volume constraint. Energy vs volume data points were obtained in intervals of 2−10 Å^3 and were subsequently fitted to a cubic spline. The respective pressure was calculated according to the derivative $p = -dE/dV$. The corresponding enthalpy was subsequently calculated according to $H = E + pV$. All calculations were performed for zero temperature.

Band structures and DOS were plotted with the "p4vasp" package[45] and the respective Fermi levels were always set to 0 eV. High symmetry points of the irreducible Brillouin zone were defined according to Bradley and Cracknell.[46] The unit for the DOS is "number of states per unit cell and eV". The choice of Wigner−Seitz radii for projected DOS was difficult, as $BaReH_9$ has both ionic and covalent character. In particular, a hard sphere model cannot account for all the electrons within the ReH_9 units (similar problems were encountered by Singh et al.[15]). This leads to the projected DOS being significantly non-normalized. As there is no unambiguous way to define Wigner−Seitz radii, projected DOS results are only qualitative in nature. Our choice of Wigner−Seitz radii was oriented along the atomic radii given in the PAW potentials, except for a slightly increased hydrogen radius to reflect the anionic character of most species: r(Ba) = 1.98 Å, r(Re) = 1.43 Å, r(H) = 0.57 Å.

For extended Hückel calculations we used the CACAO98 software package.[47] DFT calculations on discrete molecules were performed with the Gaussian 03 software package using the B3LYP hybrid functional.[48] For the description of rhenium, the SDD basis set with associated effective core potential was augmented by an f-function with the exponent $\alpha = 0.869$.[49] For hydrogen, the 6-311++G** basis set was employed. VASP was occasionally also used for DFT calculations on discrete molecules.[50] In such cases, the unit cell must be chosen large enough (6−8 Å), so that molecules do not interact with each other. Calculations were then performed for the Γ-point of the Brillouin zone only.

Acknowledgment. We are grateful to the National Science Foundation for its support of the research at Cornell by Grant CHE-0613306. G.M. thanks Professors Lorenz Cederbaum and Henning Hopf for encouragement; financial assistance was provided by the Studienstiftung des deutschen Volkes and a NRW Undergraduate Science Award. Ji Feng and Paulina Gonzalez-Morelos are acknowledged for helpful discussions.

Supporting Information Available: Crystallographic coordinates at representative pressures; additional data for NiAs-type structure, distortions of NiAs-type structure, rhombohedral structure, trigonal structure, and H_2-containing structures; calculation on H_2 elimination from molecular ReH_9^{2-}; data on hypothetical structures; comparison with LDA results; complete ref 48. This material is available free of charge via the Internet at http://pubs.acs.org.

JA908345E

(41) Zupan, A.; Blaha, P.; Schwarz, K.; Perdew, J. P. *Phys. Rev. B* **1998**, *58*, 11266–11272.
(42) Blöchl, P. E. *Phys. Rev. B* **1994**, *50*, 17953–17979.
(43) Kresse, G.; Joubert, D. *Phys. Rev. B* **1999**, *59*, 1758–1775.
(44) Monkhorst, H. J.; Pack, J. D. *Phys. Rev. B* **1976**, *13*, 5188–5192.
(45) Dubay, O. http://cms.mpi.univie.ac.at/odubay/p4vasp_site/news.php (accessed May 28, 2009).
(46) Bradley, C. J.; Cracknell, A. P. *The Mathematical Theory of Symmetry in Solids*; Clarendon Press: Oxford, 1972.
(47) Mealli, C.; Proserpio, D. M. *J. Chem. Educ.* **1990**, *67*, 399.
(48) Frisch, M. J., *Gaussian 03, Revision C. 02*; Gaussian, Inc.: Wallingford CT, 2004.
(49) Ehlers, A. W.; Böhme, M.; Dapprich, S.; Gobbi, A.; Höllwarth, A.; Jonas, V.; Köhler, K. F.; Stegmann, R.; Veldkamp, A.; Frenking, G. *Chem. Phys. Lett.* **1993**, *208*, 111–114.
(50) Sun, G.; Kurti, J.; Rajczy, P.; Kertesz, M.; Hafner, J.; Kresse, G. *J. Mol. Struct.* **2003**, *624*, 37–45.